Engineering quantum anomalous/valley Hall states in graphene via metal-atom adsorption: An *ab-initio* study

Jun Ding,[1] Zhenhua Qiao,[2,*] Wanxiang Feng,[1] Yugui Yao,[3,1,*] and Qian Niu[2,4,†]

[1]*Institute of Physics, Chinese Academy of Sciences, Beijing 100190, China*

[2]*Department of Physics, The University of Texas at Austin, Austin, Texas 78712, USA*

[3]*School of Physics, Beijing Institute of Technology, Beijing 100081, China*

[4]*International Center for Quantum Materials, Peking University, Beijing 100871, China*

We systematically investigate the magnetic and electronic properties of graphene adsorbed with diluted $3d$ transition and noble-metal atoms using first-principles calculation methods. We find that most transition-metal atoms (i.e., Sc, Ti, V, Mn, Fe) favor the hollow adsorption site, and the interaction between magnetic adatoms and the π orbital of graphene induces sizable exchange-field and Rashba spin-orbit coupling, which together open a nontrivial bulk gap near the Dirac $K/K'(\Gamma)$ points in the 4×4 (3×3) supercell of graphene leading to the quantum anomalous Hall effect. We also find that the noble-metal atoms (i.e., Cu, Ag, Au) prefer the top adsorption site, and the dominant inequality of the AB sublattice potential opens another kind of nontrivial bulk gap exhibiting the quantum-valley Hall effect in the 4×4 supercell of graphene.

I. INTRODUCTION

After an initial rush[1] since its first experimental exfoliation,[2] graphene research has turned toward the application of graphene-based electronics.[1,3] Graphene itself is a zero-gap semiconductor characterized by the linear Dirac-type dispersion, which is closely related to many amazing properties, for example, high electron mobility and half-integer quantum Hall effect (per spin and valley). However, a band gap in graphene is highly desirable for designing semiconductor devices. So far, there are several proposals for engineering a band gap, such as by employing a staggered AB sublattice potential,[4] strain effect,[5] intrinsic spin-orbit coupling[6] in single-layer graphene, or applying a perpendicular electric field in bilayer graphene.[7]

Graphene is also considered as a promising candidate for spintronics, which generally require imbalanced spin-up and -down carrier populations. However, the pristine graphene is nonmagnetic, and one needs to employ external methods to magnetize it, for example, by decorating hydrogen, sulfur, or metal adatoms on graphene[8–10] or substituting metal impurities for carbon atoms in graphene.[11] Alternatively, spin-orbit coupling is thought to be another source for manipulating spin degrees of freedom through electric means.[12] In graphene there are two kinds of spin-orbit couplings: intrinsic and extrinsic.[6] The former one has been shown to be unrealistically weak.[13] The latter one, which is also known as Rashba spin-orbit coupling, arises from the top-bottom layer symmetry breaking due to the presence of a substrate or strong perpendicular electric field, and is reported to be remarkably large in graphene placed on top of Ni(111) surface.[14]

In this article, we present a systematic investigation on the magnetic and electronic properties of graphene adsorbed with $3d$ transition and noble-metal atoms including the spin-orbit coupling using first-principles calculation methods. Our numerical results show that most transition-metal atoms favor the *hollow* adsorption site, while the noble-metal atoms prefer the *top* adsorption site. We find that both types of adsorption on graphene can give rise to bulk band gaps. Further Berry-phase effect analysis[15] demonstrates that the resulting bulk band gaps

are nontrivial and their origins are completely distinct; that is, one arises from the joint effect of exchange field and Rashba spin-orbit coupling leading to the quantum anomalous Hall effect in both 3×3 and 4×4 supercells of graphene, while the other one occurs only in the 4×4 supercell of graphene and originates from the inequality of the AB sublattice potential resulting in the quantum-valley Hall effect. Our findings should not only provide new schemes to engineer the bulk band gaps in graphene, but also show high possibility of realizing the long-sought quantum anomalous Hall effect and the dissipationless valleytronics.

II. COMPUTATIONAL METHODS

To simulate the diluted metal atoms adsorption on top of the graphene sheet, we adopt the structures of 3×3 and 4×4 supercells of graphene per metal adatom.[16] As illustrated in Figs. 1(a) and 2(a), a supercell is composed of $2N^2$ ($N = 3,4$) carbon atoms and one metal atom. The single metal atom has three possible adsorption sites: hollow (H), top (T), and bridge (B). Figures 1(b) and 2(b) plot the corresponding Brillouin zone of the 4×4 and 3×3 supercells comparing to that of the 1×1 supercell. One can notice that K^4 and K'^4 valley indices in the 4×4 supercells are well separated and thus good quantum numbers, but that those in 3×3 are folded into the Γ^3 point and are indistinguishable. For simplicity, we omit all the superscripts of high symmetry points K^4, K'^4, Γ^3, and Γ^4 in the following.

The first-principles calculations are performed using the projected-augmented-wave method[17] as implemented in the Vienna Ab-initio Simulation Package (VASP).[18] The generalized gradient approximation (GGA) exchange-correlation functional[19] is mainly used except those specified by the local density approximation (LDA) in Table I. The kinetic energy cutoff is set to be 500 eV, and the experimental lattice constant of graphene $a = 2.46$ Å is used. During the structure relaxation, all atoms are allowed to relax along the normal direction of graphene and all parameters are chosen to converge the forces to less than 0.01 eV/Å. The first

TABLE I. Energetic and structural properties of 12 metal atoms located at the lowest energy adsorption sites on the 3×3 and 4×4 supercells of graphene. The properties listed include the favored adsorption sites, adatom-graphene distance d (Å), adsorption energy δE (eV/atom), bulk band gap Δ (meV), charge transfer δQ (e) from adatom to graphene, and the magnetization of the adatoms μ_{ag} (μ_B) on the 4×4 supercell of graphene. For comparison, the data inside the parentheses are for the hollow adsorption sites, which are not the lowest energy adsorption state. 0.0* means that the global bulk band gap is zero, but the local bulk gap is finite around K/K' points for the 4×4 supercell or Γ points for the 3×3 supercell.

Atom	| 3×3 Supercell of graphene				| 4×4 Supercell of graphene				
	Site	d	δE	Δ	δQ	Site	d	δE	Δ	δQ	μ_{ag}
Sc	H	1.92	1.26	2.5	0.97	H	1.97	1.43	2.5	0.89	2.30
Ti	H	1.86	1.76	0.0*	0.88	H	1.86	1.75	1.4	0.87	3.41
V	H	1.89	0.94	0.0*	0.67	H	1.87	1.01	2.2	0.71	4.51
Cr	B(H)	2.33(2.17)	0.14(0.13)	0.0(0.0*)	0.35(0.41)	B(H)	2.37(2.15)	0.16(0.15)	0.0*(2.5)	0.37(0.45)	5.64(5.52)
Mn	H	2.07	0.14	4.5	0.56	H	2.09	0.14	4.5	0.57	5.42
Fe	H	1.56	0.98	0.0*	0.81	H	1.56	0.95	5.5	0.81	1.97
Co	H	1.55	1.31	0.0*	0.63	H	1.53	1.67	0.0*	0.66	0.99
Ni	H	1.58	1.37	60	0.51	H	1.58	1.39	0.0	0.52	0.00
Cu	T(H)	2.24(2.17)	0.24(0.10)	0.7(0.4)	0.16(0.14)	T(H)	2.25(2.17)	0.25(0.10)	38.8(7.0)	0.15(0.15)	0.90(0.92)
Zn	H	3.78	0.03	0.6	0.02	H	3.78	0.02	0.0	0.02	0.00
(LDA)	H	3.04	0.14	13.9	0.03	H	3.02	0.14	0.0	0.03	0.00
Au	T(H)	3.13(3.47)	0.14(0.13)	0.0*(2.9)	−0.08(−0.09)	T(H)	3.45(3.54)	0.16(0.16)	0.6(1.7)	−0.02(−0.15)	0.84(0.84)
(LDA)	T(H)	2.37(2.43)	1.20(0.94)	9.4(2.0)	−0.06(−0.05)	T(H)	2.40(2.52)	0.77(0.50)	161.4(8.6)	−0.09(−0.09)	1.03(0.96)
Ag	T(H)	3.57(3.69)	0.03(0.03)	0.0(1.5)	0.04(0.02)	T(H)	3.49(3.58)	0.03(0.03)	3.0(2.3)	0.02(0.02)	1.00(1.00)
(LDA)	T(H)	2.45(2.52)	0.82(0.76)	2.8(6.8)	0.08(0.07)	T(H)	2.44(2.51)	0.38(0.31)	21.8(8.7)	0.11(0.08)	0.87(0.93)

Brillouin-zone integration is carried out by using the $12 \times 12 \times 1$ and $6 \times 6 \times 1$ Monkhorst-Pack grids for the 3×3 and 4×4 supercells, respectively. A vacuum buffer space of 15 Å is set to prevent the interaction between adjacent slabs.

III. ADSORPTION ANALYSIS

Table I summarizes the stable adsorption sites, energetic and structural properties of the 3×3 and 4×4 supercells of graphene adsorbed with 12 kinds of $3d$-transition and noble-metal atoms. The stable adsorption site, distance d between adatom and graphene sheet, and the magnetization of adatoms μ_{ag} are obtained by only considering the magnetization, while other quantities are calculated by further including the spin-orbit coupling. The adsorption energy is defined as

$\delta E = E_a + E_g - E_{ag}$, where E_a, E_g and E_{ag} are the energies of the isolated metal atom, the $N \times N$ supercell of graphene, and the adatom-$N \times N$ supercell of graphene, respectively. The charge transfer δQ is calculated based on the Bader charge analysis.[20]

For clear demonstration of the resulting properties from adsorption, we divide the metal atoms into two groups.

(a) For the $3d$-transition-metal adatoms, we observe that most of them except Cr favor the hollow adsorption site. (i) For Sc, Ti, V, Fe, Co, and Ni, the adsorption distances d are very short (less than 2 Å) and the adsorption energy δE and the charge transfer are very large, which together indicate a strong hybridization. (ii) For Cr and Mn, the adsorption distance is slightly larger than 2 Å, the adsorption energy is relatively weak but the charge transfer is still
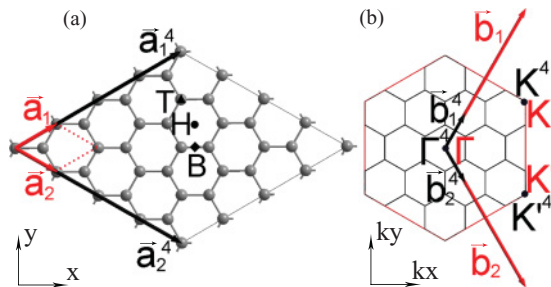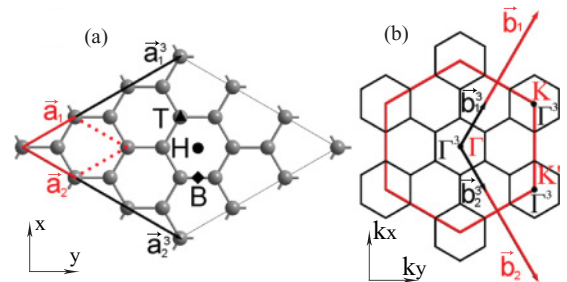

FIG. 1. (Color online) (a) A 4×4 supercell of graphene. $\vec{a}_{1,2}$ ($\vec{a}_{1,2}^4$) indicates the primitive vectors for the 1×1 (4×4) supercell. Three possible adsorption sites of single adatom on graphene are labeled as follows: hollow (H), top (T), and bridge (B). (b) Corresponding reciprocal momentum space structures: $\vec{b}_{1,2}$ ($\vec{b}_{1,2}^4$) denotes the reciprocal primitive vectors for the 1×1 (4×4) supercell. K (K^4), K' (K'^4), and Γ (Γ^4) are the high symmetry points for the 1×1 (4×4) supercell. Note that K (K^4) and K' (K'^4) are separated and thus distinguishable.

FIG. 2. (Color online) (a) A 3×3 supercell of graphene. $\vec{a}_{1,2}$ ($\vec{a}_{1,2}^3$) indicates the primitive vectors for the 1×1 (3×3) supercell. Three possible adsorption sites of single adatom on graphene are labeled as follows: hollow (H), top (T), and bridge (B). (b) Corresponding reciprocal momentum space structures: $\vec{b}_{1,2}$ and $\vec{b}_{1,2}^3$ are for reciprocal vectors for the the 1×1 and 3×3 supercells, respectively. K and K' points for the 3×3 supercell of graphene are folded into the Γ point.

remarkably large, which corresponds to a moderately weak adsorption. (iii) For Zn, the large adsorption distance and extremely small adsorption energy and charge transfer signal an extremely weak hybridization. In the following, we show that the reconstruction of the electronic configurations of the adsorbed metal atoms is intimately dependent on the strength of adsorption on the graphene sheet.

In Table I, we notice that the magnetic moments of adatoms μ_{ag} are greatly altered compared to that of the isolated atoms. They are found to obey the following rules. (1) When the $3d$ shell is less than half filled (i.e., Sc, Ti, V), the strong hybridization lowers the energy of the $3d$ orbital. This makes the $4s$ electrons transfer to the unoccupied $3d$ orbital. Since the resulting $3d$ shell is not over half filled, the Hund's rule dictates that all the $3d$ electrons possess the same spin polarization leading to the increase of the magnetic moments μ_{ag} of the adsorbed metal atom. (2) When the $3d$ shell is exactly half filled (i.e., Cr, Mn), the moderately weak adsorption hardly affects the $3d$-orbital energy during the hybridization. Based on the Hund's rule, all $3d$ electrons are equally spin polarized showing a maximum magnetization. In the influence of the high magnetization from the $3d$ shell, the $4s$ electrons tend to align with the spin of the $3d$ electrons, which slightly increases the magnetic moment. (3) When the $3d$ shell is over half filled (i.e., Fe, Co, Ni), the strong hybridization lowers the $3d$-shell energy and the electron transfer from the $4s$ orbital to the $3d$ orbital decreases the magnetic moment due to the occupying of the unpaired $3d$ orbital.[9] In particular, for Ni the two $4s$ electrons are transferred to the $3d$ orbital and form a closed $3d$ shell, giving rise to a vanishing magnetic moment. (4) For atoms with closed $3d$ and $4s$ shells (i.e., Zn), they behave like an inert atom leaving graphene nearly unaffected.

(b) For the noble-metal adatoms (i.e., Cu, Ag, Au), we find that they are stable at the top adsorption site. Consistent with Ref. 9, the long adsorption distance, low adsorption energy, and weak charge transfer originate from the physical adsorption involving the van de Waals forces. In Table I, we also provide the LDA results for Au and Ag adsorption. The major differences are that the adsorption distance d is dramatically decreased and the adsorption energy δE is largely increased. Because of the closed d shells, the single s valence electron contributes to the magnetic moment $\mu_{ag} \sim 1\mu_B$.

Due to the magnetic proximity effect from the magnetic adatoms, graphene could be magnetized. In the absence of spin-orbit coupling, for the 4×4 supercell of graphene we estimate the induced exchange field[21] near the Dirac points (K and K') to be $\lambda = 145$ (Sc), 277 (Ti), 199 (V), 359 (Cr), 181 (Mn), 57 (Fe), 462 (Co), 0 (Ni), and 23 (Cu) in units of meV for the hollow-site adsorption, while for the 3×3 supercell of graphene, the induced exchange field near Γ point is calculated to be $\lambda = 213$ (Sc), 432 (Mn), 1080 (Fe), 442 (Co), and 0 (Ni) in units of meV for the hollow-site adsorption.

IV. BAND STRUCTURES AND BERRY CURVATURES ANALYSIS

A. Adsorption on 4×4 supercell of graphene

We classify the 12 kinds of atoms into three groups: (1) atoms (e.g., Sc, Mn, Fe) adsorbed at the hollow site, and graphene is magnetized; (2) atoms (e.g., Ni) adsorbed at the
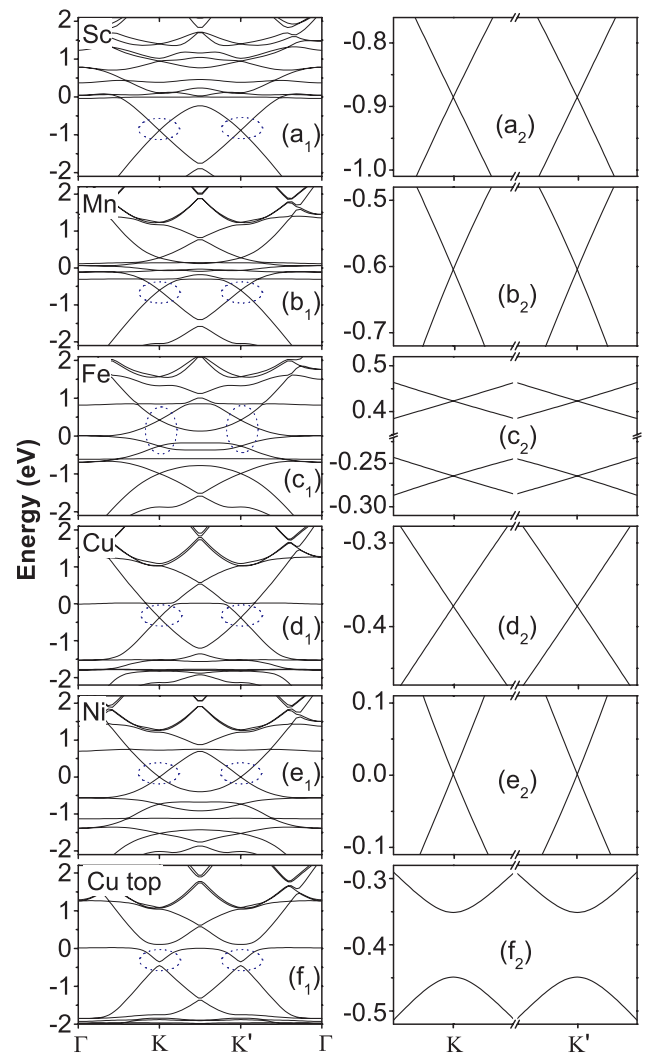

FIG. 3. (Color online) Left column (a_1)–(e_1): Full bulk band structures based on GGA for Sc (a_1), Mn (b_1), Fe (c_1), Cu (d_1), and Ni (e_1) adsorbed at the hollow site on a 4×4 supercell of graphene along high symmetry lines without involving spin degrees of freedom. (f_1) Full bulk band structure based on GGA for Cu adsorbed at top site on a 4×4 supercell of graphene. Right column (a_2)–(e_2): Magnification of the bands of panels (a_1)–(e_1) around K and K' Dirac points showing linear dispersion. (f_2) Magnification of the bands panel (f_1) with an obvious bulk band gap opening.

hollow site, but graphene is not magnetized; (3) atoms (e.g., Cu) adsorbed at the top site.

Figure 3 plots the band structures of adatom-graphene for (a) Sc, (b) Mn, (c) Fe, (d) Cu, and (e) Ni adsorbed at the *hollow* sites and (f) Cu adsorbed at the *top* site on the 4×4 supercell of graphene in the absence of spin degree of freedom. Panels (a_1)–(f_1) exhibit the full bulk bands along the high symmetry lines, and panels (a_2)–(f_2) magnify the bands near the Dirac points K and K'. One can see that panels (a_2)–(e_2) show clear linear Dirac dispersion at K and K' points, while in panel (f_2) a bulk band gap opens at K and K' points, which will be shown later to be a nontrivial gap exhibiting the quantum valley-Hall state.

As shown in Fig. 4, when the magnetization is further included, one can find that the doubly degenerate bands
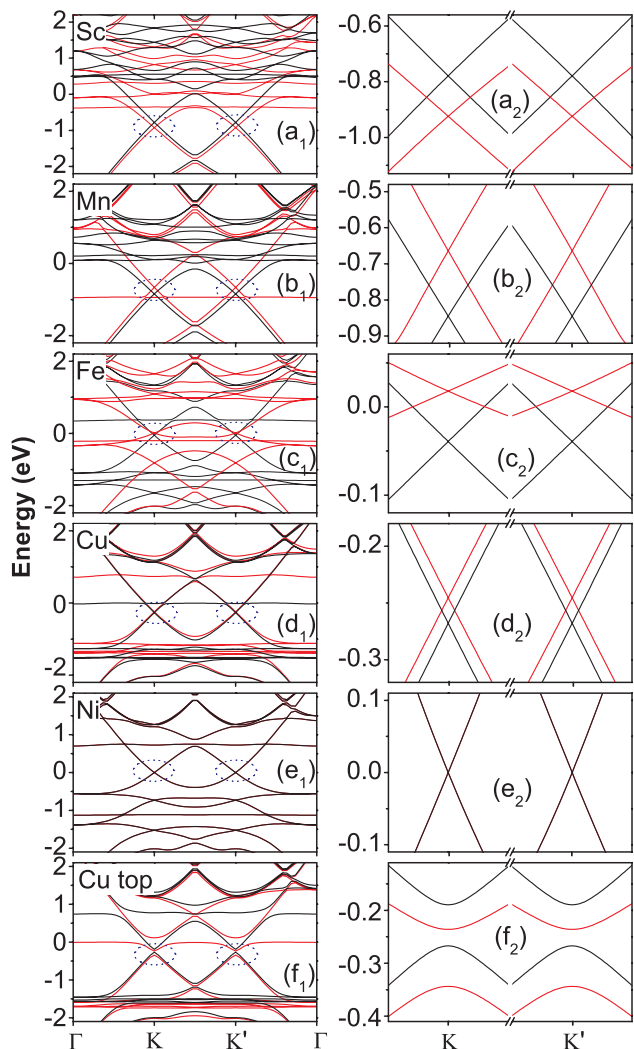
FIG. 4. (Color online) Left column (a₁)–(e₁): Full bulk band structures based on GGA for Sc (a₁), Mn (b₁), Fe (c₁), Cu (d₁), and Ni (e₁) adsorbed at the hollow site on a 4 × 4 supercell of graphene along high symmetry lines by including the magnetization. (f₁) Full bulk band structure based on GGA for Cu adsorbed at top site on a 4 × 4 supercell of graphene. Right column (a₂)–(f₂): Magnification of the bands around K and K' Dirac points. Red and black are used to denote spin-up and spin-down bands.
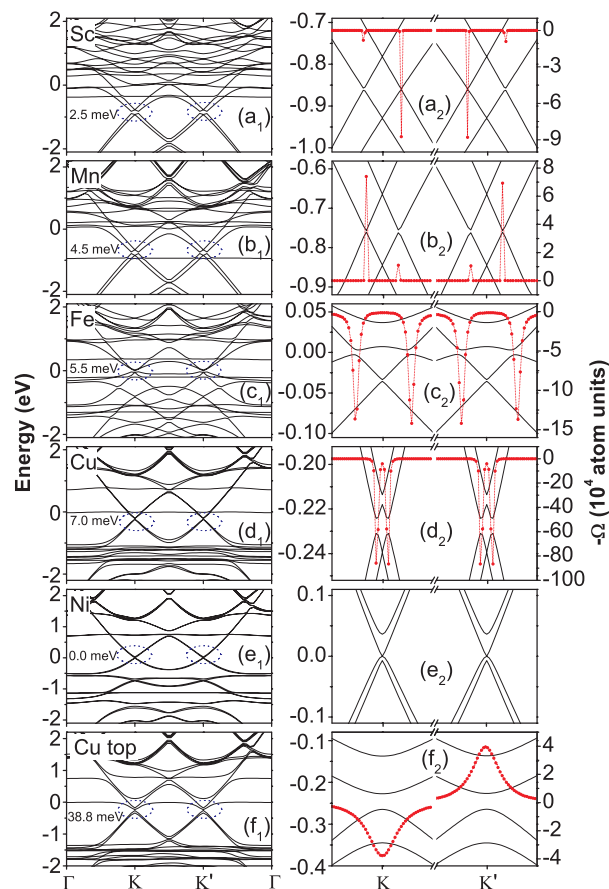

FIG. 5. (Color online) Left column (a₁)–(e₁): Full bulk band structures based on GGA for Sc (a₁), Mn (b₁), Fe (c₁), Cu (d₁), Ni (e₁) adsorbed at the hollow site on a 4 × 4 supercell of graphene along high symmetry lines by including the spin-orbit coupling. (f₁) Full bulk band structure based on GGA for Cu adsorbed at top site on a 4 × 4 supercell of graphene. Right column (a₂)–(f₂): Magnification of the bands around K and K' Dirac points (in black), and the Berry curvatures $\Omega(\mathbf{k})$ for the whole valance bands (in red).

become spin-split (i.e., we use red and black to denote spin-up and spin-down bands) for the magnetic adatoms, that is, Sc, Mn, Fe, Cu, Cu-top. For Ni adsorption, due to the vanishing magnetic moment of Ni after the hybridization with graphene, the introduction of magnetization leaves the band structure unaffected. From panels (a₂)–(d₂) of the magnetic adatom adsorbed on the hollow site of graphene, we observe that there are four crossing points arisen from the relative shift between spin-up and spin-down bands around either K or K' point. In panels (f₂) for the Cu adsorption on the top site of graphene, the magnetization-induced spin-shift decreases the original bulk gap.

The above discussions have been more or less mentioned in some previous work.[9] However, the following part with spin-orbit coupling being considered is the first time to be addressed. Our main contribution of this work is to explore the

possibility of engineering the topological states in graphene proposed in Ref. 22 through the adsorption of magnetic atoms on top of graphene.

Figure 5 plots the band structures with both magnetization and spin-orbit coupling being tuned on in the calculation. Through comparing the band structures with and without spin-orbit coupling in Figs. 4 and 5, we see that sizable bulk band gaps open at K and K' Dirac points in panels (a₂)–(d₂), where spin-up and spin-down bands are crossing due to the introduction of magnetization. The presence of such a bulk band gap signals an insulating state. However, we note that all the Fermi levels lie outside the bulk gaps except that in panel (c₂) for Fe adsorption. Therefore, to realize these insulators one has to artificially adjust the Fermi levels to be inside the gap, for example, by applying a gate voltage.

To further identify the nontrivial topological properties of the obtained insulators, we turn to the Berry phase analysis in the momentum space.[15] By constructing the Bloch wave functions ψ from the self-consistent potentials, the

Berry curvature $\Omega(\boldsymbol{k})$ can be obtained using the following formula:[23–25]

$$\Omega(\boldsymbol{k}) = \sum_n f_n \Omega_n(\boldsymbol{k}),$$

$$\Omega_n(\boldsymbol{k}) = -\sum_{n' \neq n} \frac{2\mathrm{Im}\langle \psi_{n\boldsymbol{k}} | v_x | \psi_{n'\boldsymbol{k}} \rangle \langle \psi_{n'\boldsymbol{k}} | v_y | \psi_{n\boldsymbol{k}} \rangle}{(\omega_{n'} - \omega_n)^2},$$

(1)

where the summation is over all n valence bands below the bulk band gap, f_n is the Fermi-Dirac distribution function, $\omega_n \equiv E_n/\hbar$, and $v_{x(y)}$ is the velocity operator. In Figs. 5(a$_2$)–5(d$_2$) and 5(f$_2$), we also plot the Berry curvatures $-\Omega(\boldsymbol{k})$ in dotted curves along the high symmetry lines. One can observe that the nonzero Berry curvatures are mainly distributed around the K and K' points. In particular, the Berry curvatures Ω in panels (a$_2$)–(d$_2$) around the K point share the same sign as that near the K' point. The Chern number can be obtained by integrating the Berry curvatures Ω over the first Brillouin zone using Eq. (2). Our data show that $\mathcal{C} = +2$ for the insulating state of Sc, Fe, Cu adsorption on graphene, while $\mathcal{C} = -2$ for the insulating state of the Mn adsorption,

$$\mathcal{C} = \frac{1}{2\pi} \int_{\mathrm{BZ}} d^2 k \, \Omega.$$

(2)

The nonvanishing Chern number $\mathcal{C}$ in the absence of magnetic field signifies a quantum anomalous Hall (QAH) effect. This was first theoretically proposed by Haldane in a Honeycomb toy model after the experimental observation of the integer quantum Hall effect in 1980s,[26] but yet observed in experiment. Until recently, it resurges with several other theoretical proposals.[22,27] In the subsequent section, we analyze the mechanism of the formation of the QAH state in graphene.

Figure 5 clearly shows that the group (1) adatoms (magnetic adatoms adsorbed on the hollow site) can open a nontrivial bulk band gap and achieve the QAH effect, but group (2) adatoms (nonmagnetic adatoms adsorbed on the hollow site) cannot. Therefore, we conclude that the magnetization of graphene, which breaks the time-reversal symmetry, is an essential ingredient of the resulting QAH effect. Alternatively, in Fig. 4 we find that no bulk band gap opens for the group (1) atom-adsorption when the spin-orbit coupling is switched off. This makes the spin-orbit coupling be the other key ingredient of the QAH effect.

As mentioned in the Introduction, there are two types of spin-orbit coupling. One is intrinsic spin-orbit coupling, and the other one is Rashba spin-orbit coupling. From Table I, we notice that there is substantial charge transfer δQ from the $3d$ orbital of metal adatoms to π orbital of graphene. Due to the asymmetry of the adatom-4×4 supercell of graphene structure, a sizable potential gradient is formed at the interface, which induces a considerable Rashba spin-orbit coupling.[14] Therefore, based on the qualitative analysis one can determine that it is the Rashba-type spin-orbit coupling that plays a crucial role in the formation of QAH effect.

Panel (d$_2$) for Cu adsorption at the hollow site further supports that the spin-polarized electron transfer from $4s$ orbital to graphene can also realize the QAH state. Thus, we summarize that the realization of the QAH state is only *dependent* on the spin-polarized charge transfer, but *independent* of the details of the adsorption (i.e., strong or weak hybridization, charge transfer from the $4s$ or $3d$ orbital). Although the induced Rashba spin-orbit coupling and magnetization in graphene are nonuniformly distributed in the supercell structure, the gap opening mechanism near the Dirac points is exactly the same as that proposed in the tight-binding model with uniformly distributed Rashba spin-orbit coupling and magnetization:[22] First, the magnetization lifts the spin-up and -down bands, accompanying the bands crossing; second, the Rashba spin-orbit coupling opens a bulk gap at the bands crossing points. In this sense, we have provided a more realistic method (i.e., doping $3d$ transition-metal atoms on the hollow site of 4×4 supercell of graphene) to implement the theoretically predicted QAH state in graphene.

For the noble-metal adatoms, because of the Van de Vaals force they favor the top adsorption site. Besides, the Rashba spin-orbit coupling resulted from asymmetry and the exchange field from magnetic proximity, the major difference from the hollow-site adsorption is the extra introduction of the inequality of AB-sublattice potential, which breaks the spatial inversion symmetry. For example, we have considered the case with Cu adsorbed at the top site as shown in the panel (f$_2$). Through plotting the Berry curvature distribution, we observe that Ω around the K point exhibits opposite sign as that near the K' point. This strongly indicates a quantum valley-Hall (QVH) state[4,28,29] with canceling Chern numbers, that is, $\mathcal{C} = 0$, but $\mathcal{C}_K = -\mathcal{C}_{K'} = 1$. We can attribute this result to the dominating role of the AB sublattice inequality that suppresses the joint effect from Rashba spin-orbit coupling and exchange field.

B. Adsorption on the 3 × 3 supercell of graphene

In Sec. IV A, we have studied the electronic structures of adatom-4×4 supercell of graphene, in which K and K' are valley separated, and we can capture rich physics arising from these Dirac points. As a special case, the adsorption on the 3×3 supercell of graphene has rarely been studied due to the mixing of K and K' valleys. In the following, we address such a question: whether the 3×3 supercell of graphene is still able to host the QAH state or not. This is because in experiment it is difficult to artificially dope the adatoms into some particular periodic pattern, that is, 4×4 supercells. In contrast, the randomly diluted metal adatoms may form the unwilling 3×3 supercell to some degree. Therefore, it is a more practical issue to address the possibility of realizing the QAH state in the 3×3 supercell of graphene.

In this section, we only study the metal atom adsorption on the hollow site of the 3×3 supercell of graphene, because it is meaningless to search for the QVH state in the absence of a valid definition of valley degree of freedom. In the following discussion, we only show the electronic structures for several representative adatoms, that is, Sc, Mn, Fe, Co, Ni, and Cu.

Figure 6 exhibits the band structures of 3×3 supercells of graphene adsorbed with (a) Sc, (b) Mn, (c) Fe, (d) Cu, (e) Ni, and (f) Co adatoms on top of the hollow position without involving spin degrees of freedom, that is, nonmagnetic calculation. In panels (a$_1$)–(f$_1$), we plot the full band structures along the high symmetry lines. From the band structures shown in panels (a$_2$)–(f$_2$), the magnification of the circled bands in
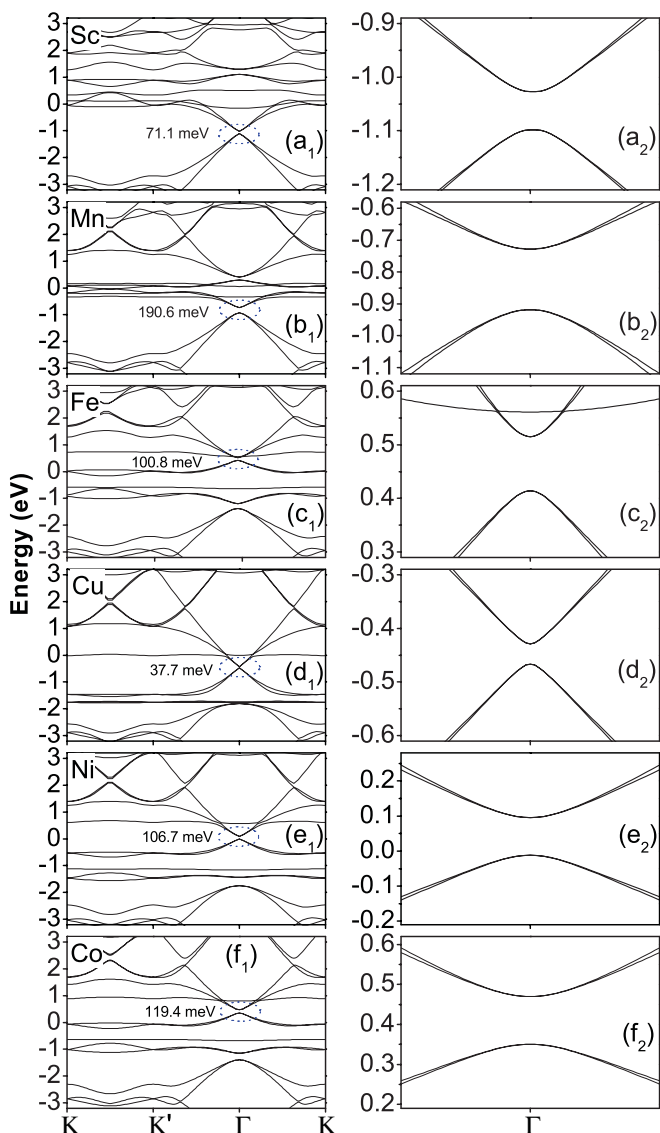
FIG. 6. (Color online) Left column (a_1)–(f_1): Full band structures of adatom-3×3 supercell of graphene for Sc, Mn, Fe, Cu, Ni, and Co adsorbed on top of the hollow position without including magnetization and spin-orbit coupling along the high symmetry line. Right column (a_2)–(f_2): Magnification of the circled bands around Γ point in panels (a_1)–(f_1). Bulk band gaps are opened at the Γ point due to the intervalley scattering effect. Note that there are two equivalent band gaps at Γ point except in the band structure of Cu adsorption.

the left column, we observe that large band gaps can open at the Γ point due to the inter-valley scattering between K and K', that is, $\Delta = 71.1, 190.6, 100.8, 37.7, 106.7, 119.4$ in units of meV for the 3×3 supercell of graphene adsorbed with Sc, Mn, Fe, Cu, Ni, and Co, respectively. This is completely distinct from that of the adsorption on the 4×4 supercells of graphene, where the perfect Dirac-cone dispersion holds at both K and K' points. Note that in the calculations we have used the hydrogen atom to saturate the dangling bond of Mn atom, because in the Mn adsorption the dangling d band is properly located inside the resulting bulk gap. In the first column of Fig. 6 one can see that there are two clear bulk band gaps opening at the Γ points for Sc, Mn, Fe, and Cu adsorption.
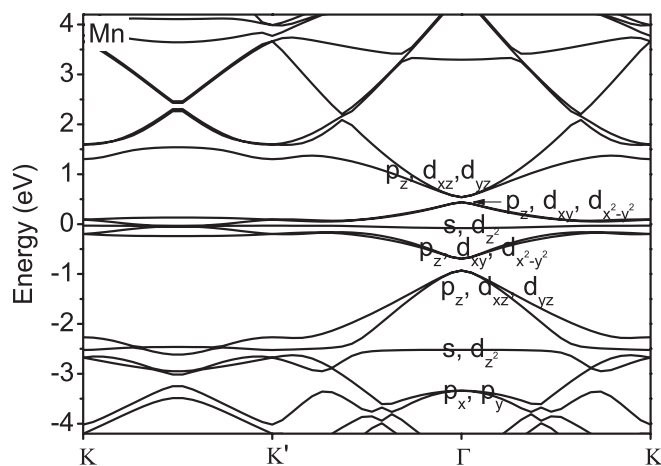

FIG. 7. Projected bands analysis for the bands near the two bulk band gaps in Fig. 6(b_1). We can see that the bands near the two bulk gaps possess the same orbital components.

From the projected band analysis of Mn adsorption as plotted in Fig. 7, we show that the two bulk band gaps are essentially equivalent by constructing from the same orbital components of P_z, d_{xz}, and d_{yz} (or P_z, d_{xy}, and $d_{x^2-y^2}$).

Similar to the adsorption on the 4×4 supercell of graphene, when the magnetization is included, the spin-up (-down) bands are upward (downward) shifted (see Fig. 8). This results in three possible results: (i) As plotted in panels (a_2)–(c_2) and (f_2) for Sc, Mn, Fe, and Co adsorption, the induced magnetization is so large that the original bulk band gaps from the intervalley scattering are closed due to the crossover between the spin-down bands from the conduction bands and the spin-up bands from the valence bands. (ii) For panel (d_2) of Cu adsorption, the magnetization is moderately large (i.e., $\lambda = 0.035$ eV) that the original bulk band gaps are just decreased but not closed. (iii) For the Ni adsorption in panel (e_2) the band structure is exactly the same as that shown in Fig. 6 (e_2) because graphene is not magnetized from the Ni adsorption.

When the spin-orbit coupling is further switched on, we find that nontrivial band gaps can open at the crossing points between the spin-up and spin-down bands [see panels (a_2)–(c_2) and (f_2) in Fig. 9], which shows similar origin as that in the adsorption on the 4×4 supercells in Fig. 1. However, we find that only the bulk band gaps in panels (a_1) and (b_1) are globally opened for Sc ($\Delta = 2.5$ meV) and Mn ($\Delta = 4.5$ meV), while that for Fe and Co in panels (c_1) and (f_1) are just locally opened. Therefore, in the following, we only focus on the nontrivial topological properties for Sc and Mn adsorption. Through calculating the Berry curvatures Ω along the high symmetry lines for all the valence bands below the bulk gap, we find that all the Berry curvatures Ω share the same sign as shown in panels (a_2) and (b_2), resulting in the nonvanishing Chern number $\mathcal{C}$. By integrating all the Berry curvatures below the band gaps, our calculation shows that $\mathcal{C} = +2/-2$ for the Sc/Mn adsorption. This again signals a QAH insulating state for the energies inside the bulk gap. Since the Fermi energy is not located inside the band gap, one has to apply external gate voltage to adjust the Fermi level inside the band gap to realize the insulating state. We want to specify that though the global bulk band gaps are zero for Fe and Co adsorption, there exist
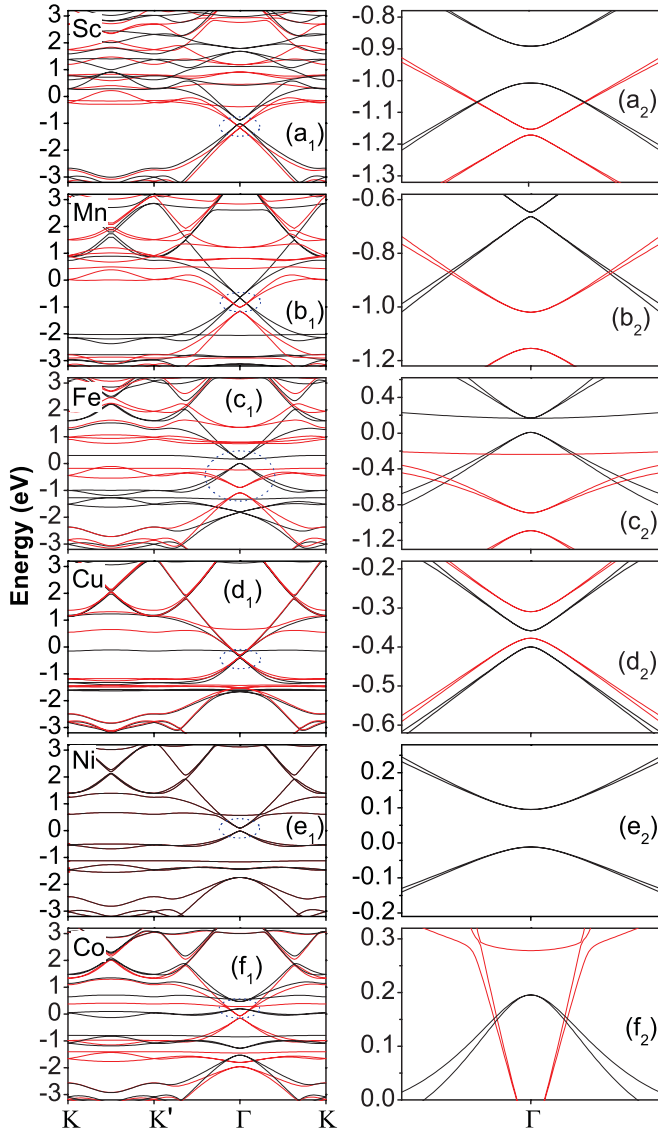
FIG. 8. (Color online) Left column (a_1)–(f_1): Full band structures of adatom-3 × 3 supercell of graphene for Sc, Mn, Fe, Cu, Ni, and Co adsorbed on top of the hollow position by including the magnetization along the high symmetry line. Right column (a_2)–(f_2): Magnification of the circled bands around Γ point in panels (a_1)–(f_1). Colors are used to distinguish the spin-up (black) and spin-down (red) bands. In the right column all the spin-up and spin-down bands are crossing due to the large magnetization except that for Cu and Ni adsorption. In panel (d_2) for Cu adsorption the magnetization is less than the original band gap amplitude; therefore, the relative shift between the spin-up and spin-down bands does not cross to close the band gap. In panel (e_2) for Ni adsorption the band structure is exactly the same as that in Fig. 6(e) because of the vanishing magnetic moment of Ni adatom.

FIG. 9. (Color online) Left column (a_1)–(f_1): Full band structures of adatom-3 × 3 supercell of graphene for Sc, Mn, Fe, Cu, Ni, and Co adsorbed on top of the hollow position by including both the magnetization and spin-orbit coupling along the high symmetry line. Right column (a_2)–(f_2): Magnification of the circled bands around Γ point in panels (a_1)–(f_1). In panels (a_2)–(c_2) and (f_2), the nontrivial bulk band gap is open at the crossing points. However, only bulk band gaps are globally opened in panels (a_2)–(b_2) for Sc and Mn adsorption, while the gaps in panels (c_2) and (f_2) are just locally opened. Therefore, only the Sc/Mn adsorbed 3 × 3 graphene structure can exhibit the nontrivial insulating properties when the Fermi level is artificially adjusted to the bulk band gaps. In addition, we also plot the total Berry curvatures Ω(k) in panels (a_2)–(b_2) for all the valence bands below the bulk band gaps.

V. DISCUSSIONS

In this article, we have used the first-principles calculation methods to investigate the spin-orbit-coupling-induced topological states in graphene. For the 3d-transition-metal adsorption on graphene, we employ the GGA exchange-correlation functional in the simulation, while for the noble-metal adsorption both GGA and LDA exchange-correlation functionals are adopted. The main contributions of this article are to demonstrate the possibility of engineering the topological states (i.e., QAH state or QVH state) and to analyze

the local band gaps, which can produce the QAH state when all the valence bands are occupied. This has been confirmed from the Chern number calculation by integrating the bands below the local band gaps. While for the other two adsorption of Cu and Ni is shown in panels (d2)–(e2), we can see that the spin-orbit coupling further decreases the bulk gaps and there is not a new topological state.
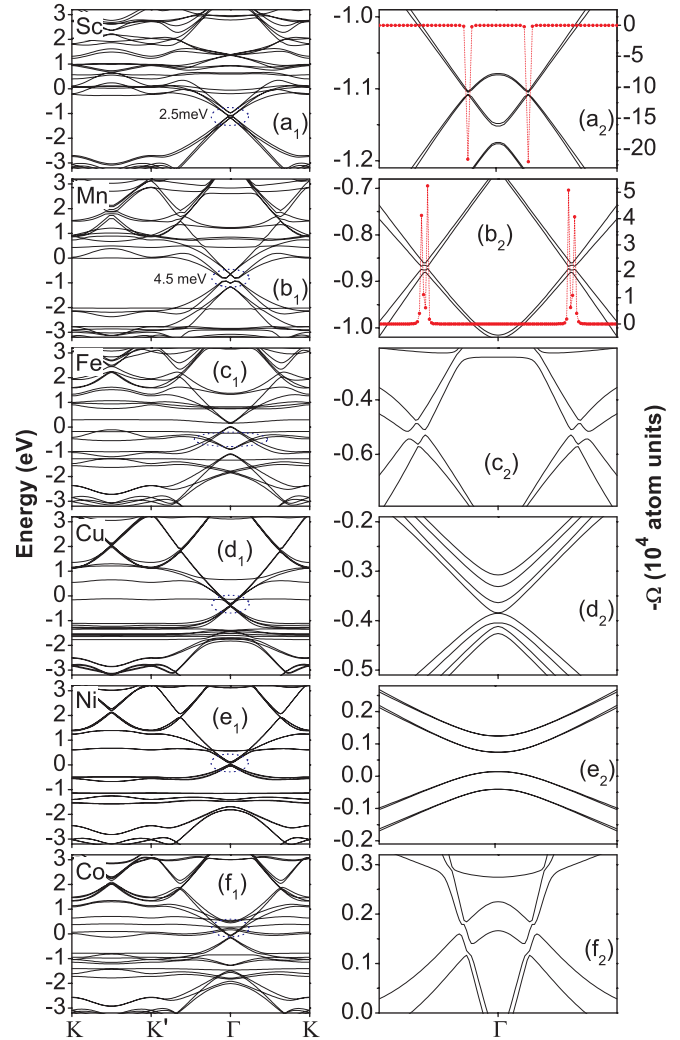
the origins of the two different topological states. For other kinds of exchange-correlation functionals, we expect that they can bring in some differences (e.g., the strength of the induced magnetization or Rashba spin-orbit coupling and the size of nontrivial bulk gap), but they will not affect the essence of the topology of the nontrivial bulk gap according to our theoretical predictions of the QAH effect[22] and QVH effect.[4] However, it is still interesting to study the dependence on the exchange-correlation functionals in the future.

From the practical view of point, though we have verified the possibility of realizing the QAH state in graphene using the first-principles calculation methods, it is still too ideal and difficult for the experimental physicists to dope the adatoms periodically. We suggest that a more realistic method to experimentally observe the QAH state should be placing graphene sheet on top of magnetic insulators or anti-ferromagnetic insulators (along the layered ferromagnetic phase).

VI. CONCLUSIONS

Using first-principles calculation methods, we study the magnetic and electronic properties of graphene adsorbed with 12 metal atoms including the spin-orbit coupling. In our simulations, we have used two kinds of supercells of graphene (3×3, and 4×4) to model the diluted metal atom adsorption. For the 4×4 supercells of graphene adsorption, we show that the QAH effect can be realized when the nontrivial bulk band gaps open by doping the magnetic adatoms (i.e., Sc, Ti, V, Mn, Fe, Cu, Ag, and Au) at the hollow site of graphene, which originates from the joint effect of the Rashba spin-orbit coupling and magnetization.[22] We also find that when the noble-metal atoms (i.e., Cu, Ag, and Au) are adsorbed at the

top site, which correspond to their lowest energy states, the QVH effect can be produced from the inversion symmetry breaking due to the inequality of the AB sublattice potential.

For the 3×3 supercells of graphene adsorbed with metal atoms on the top of hollow position, large trivial bulk band gaps can open at the Γ point due to the intervalley scattering without considering the spin degrees of freedom. As long as the magnetization of the adatoms (i.e., Sc, Mn, Fe, and Co) is large enough to close the original trivial band gap, the spin-orbit coupling is able to open nontrivial bulk band gaps around the Γ point to realize the QAH effect. This finding not only generalizes our finding of QAH effect in the 4×4 supercell to the 3×3 supercell of graphene, but also enhances the experimental feasibility of the QAH effect in graphene.

Our findings of the QAH and QVH states in the adatom-graphene systems not only provide new gap opening schemes for the industrial application, but also pave the way for the realization of the dissipationless charge/valley current in spintronics and valleytronics.

---

*zhqiao@physics.utexas.edu; ygyao@bit.edu.cn

†On leave from the University of Texas at Austin.

[1] W. J. Beenakker, Rev. Mod. Phys. **80**, 1337 (2008); A. H. Castro Neto *et al.*, *ibid.* **81**, 109162 (2009).

[2] K. S. Novoselov *et al.*, Science **306**, 666 (2004).

[3] F. Chen *et al.*, Nano Lett. **9**, 2571 (2009); Y. Zheng G. X. Ni, C. T. Toh, C. Y. Tan, K. Yao, and B. Ozyilmaz, Phys. Rev. Lett. **105**, 166602 (2010).

[4] D. Xiao, W. Yao, and Q. Niu, Phys. Rev. Lett. **99**, 236809 (2007); S. Y. Zhou *et al.*, Nat. Mater. **6**, 770 (2009).

[5] F. Guinea *et al.*, Nat. Phys. **6**, 30 (2010).

[6] C. L. Kane and E. J. Mele, Phys. Rev. Lett. **95**, 146802 (2005).

[7] J. B. Oostinga *et al.*, Nat. Mater. **7**, 151 (2008); Y. Zhang *et al.*, Nature (London) **459**, 820 (2009).

[8] Y. G. Zhou *et al.*, J. Appl. Phys. **105**, 104311 (2009); J. Zhou *et al.*, Appl. Phys. Lett. **95**, 103108 (2009); Nano Lett. **9**, 3867 (2009); O. V. Yazyev and A. Pasquarello, Phys. Rev. B **82**, 045407 (2010); O. Leenaerts, B. Partoens, and F. M. Peeters, *ibid.* **77**, 125416 (2008); H. Sevinçli, M. Topsakal, E. Durgun, and S. Ciraci, *ibid.* **77**, 195434 (2008).

[9] K. T. Chan, J. B. Neaton, and M. L. Cohen, Phys. Rev. B **77**, 235430 (2008).

[10] G. Savini, A. C. Ferrari, and F. Giustino, Phys. Rev. Lett. **105**, 037002 (2010).

[11] E. J. G. Santos, D. Sanchez-Portal, and A. Ayuela, Phys. Rev. B **81**, 125433 (2010).

[12] I. Zutic *et al.*, Rev. Mod. Phys. **76**, 323 (2004); D. Awschalom *et al.*, Physics **2**, 50 (2009).

[13] Y. G. Yao, F. Ye, X. L. Qi, S. C. Zhang, and Z. Fang, Phys. Rev. B **75**, 041401(R) (2007); H. Min, J. E. Hill, N. A. Sinitsyn, B. R. Sahu, L. Kleinman, and A. H. MacDonald, *ibid.* **74**, 165310 (2006).

[14] A. Varykhalov, A. M. Shikin, C. Biswas, E. Vescovo, A. Rybkin, D. Marchenko, and O. Rader, Phys. Rev. Lett. **101**, 157601 (2008); Y. S. Dedkov, M. Fonin, U. Rudiger, and C. Laubschat, *ibid.* **100**, 107602 (2008).

[15] D. Xiao, M.-C. Chang, and Q. Niu, Rev. Mod. Phys. **82**, 1959 (2010).

[16] The reason why we consider 3×3 and 4×4 is that they represent two different adsorption types: (1) K and K' are separated and therefore good quantum numbers; (2) K and K' are folded into the same Γ point and indistinguishable. For other lower concentrations (e.g., 5×5, 7×7), they should reach the similar results as that of 4×4 supercell with smaller bulk band gap.

[17] P. E. Blöchl, Phys. Rev. B **50**, 17953 (1994).

[18] G. Kresse and J. Furthmuller, Phys. Rev. B **54**, 11169 (1996).

[19] J. P. Perdew, J. A. Chevary, S. H. Vosko, K. A. Jackson, M. R. Pederson, D. J. Singh, and C. Fiolhais, Phys. Rev. B **46**, 6671 (1992).

[20] W. Tang *et al.*, J. Phys. Condens. Matter **21**, 084204 (2009).

[21] It is obtained from $\lambda = (\varepsilon_\uparrow - \varepsilon_\downarrow)/2$ at K/K' point.

[22] Z. H. Qiao, S. A. Yang, W. Feng, W. K. Tse, J. Ding, Y. Yao, J. Wang, and Q. Niu, Phys. Rev. B **82**, 161414(R) (2010); W.-K. Tse, Z. Qiao, Y. Yao, A. H. MacDonald, and Q. Niu, *ibid.* **83**, 155447 (2011).

[23] D. J. Thouless, M. Kohmoto, M. P. Nightingale, and M. denNijs, Phys. Rev. Lett. **49**, 405 (1982).

[24] M. C. Chang and Q. Niu, Phys. Rev. B **53**, 7010 (1996).

[25] Y. G. Yao, L. Kleinman, A. H. MacDonald, J. Sinova, T. Jungwirth, D. S. Wang, E. Wang, and Q. Niu, Phys. Rev. Lett. **92**, 037204 (2004).

[26] F. D. M. Haldane, Phys. Rev. Lett. **61**, 2015 (1988).

[27] C. X. Liu, X. L. Qi, X. Dai, Z. Fang, and S. C. Zhang, Phys. Rev. Lett. **101**, 146802 (2008); C. Wu, *ibid.* **101**, 186807 (2008); R. Yu *et al.*, Science **329**, 61 (2010); Y. Zhang and C. Zhang, Phys. Rev. B **84**, 085123 (2011).

[28] J. B. Oostinga, H. B. Heersche, X. Liu, A. F. Morpurgo, and L. M. K. Vandersypen, Nat. Mater. **7**, 151 (2007).

[29] P. Ghaemi, S. Ryu, and D.-H. Lee, Phys. Rev. B **81**, 081403(R) (2010).